Korean J. Chem. Eng., 38(5), 1043-1051 (2021)
DOI: 10.1007/s11814-021-0771-y

pISSN: 0256-1115
eISSN: 1975-7220

Comparison of carbon molecular sieve and zeolite 5A for CO_2 sequestration from CH_4/CO_2 mixture gas using vacuum pressure swing adsorption

Daeho Ko†

Process Team of Technical Division, Daesung Industrial Gases Co., Ltd.,
128, Sandan-ro, Danwon-gu, Ansan-si, Gyeonggi-do 15434, Korea
(*Received 7 December 2020 • Revised 11 February 2021 • Accepted 23 February 2021*)

Abstract−The performance of carbon molecular sieves and zeolite 5A was compared in a four-bed vacuum pressure swing adsorption process. The purpose of the process is to sequester CO_2 from a CH_4/CO_2 mixture gas, such as coal bed methane or landfill gas. This study investigated the effects of the design variables and operating variables on methane purity, recovery, and specific power through simulations of the process using the two adsorbents. The adopted design variables for the investigation are the packing bed length and the diameter of the adsorption bed, and the selected operating variables are the adsorption pressure and vacuum pressure. The simulation results show that zeolite 5A is better than carbon molecular sieve in terms of power, especially under low-pressure operating conditions with a vacuum pressure of 1,000 Pa. However, carbon molecular sieves are better in terms of purity enhancement when the vacuum pressure is higher than approximately 2,000 Pa.

Keywords: Vacuum Pressure Swing Adsorption, Carbon Molecular Sieve, Zeolite 5A, Simulation, CO_2 Sequestration

INTRODUCTION

The main cause of various environmental problems, such as an increase in sea level and global warming, is excessive greenhouse gases in the atmosphere [1]. Since the most important greenhouse gas is carbon dioxide (CO_2) [2], the sequestration of CO_2 from gases has been the main issue and is necessary for many applications to limit the greenhouse effect and associated global warming. Various technical options for the separation of CO_2 from a gas mixture stream include chemical absorption, physical absorption, adsorption, cryogenics, and membranes [3]. Amine-based absorption is a mature commercialized technology for CO_2 separation, and new concepts such as modified membranes and adsorption seem to be very promising [3].

Although the absorption process has been widely used for CO_2 sequestration in large-scale plants, pressure swing adsorption (PSA) has been adopted in comparatively medium-scale plants because PSA is regarded as an energy-efficient gas separation technology [4].

Generally, the PSA process performance is highly affected by (1) design conditions, such as the bed diameter, packing bed length, configuration, and number of beds, and (2) operating conditions, including the operating step times, gas flow rates, and operating pressure. In addition, for the design of PSA processes, a suitable adsorbent selection is particularly crucial because the adsorbent's physical properties, including selectivity, adsorption capacity, mass transfer kinetics, and adsorption heat, strongly influence the PSA performance. Thus, many researchers have studied and compared the performance of adsorbents in PSA processes as follows.

CO_2 separation from low-CO_2-concentration flue gas using activated carbon (AC) and carbon molecular sieve (CMS) as adsorbents was studied by Kikkinides et al. [5]. For the separation of CO_2 from mixture gases in PSA processes, synthetic zeolites, CMS, and AC were suggested as candidate adsorbents by Chue et al. [6]. Chue et al. also examined AC and zeolite 13X to recover high-purity CO_2 using the PSA process from two flue gases (16% and 26% CO_2 with a balance gas, N_2) [6]. The adsorption dynamics of N_2, O_2, and Ar in a kinetic separation bed with CMS and an equilibrium separation bed with zeolite 13X using dry air as the feed gas were investigated by Jee et al. [7]. Siriwardane et al. studied the volumetric gas adsorption of CO_2, N_2, and O_2 on three natural zeolites to determine the equilibrium adsorption capacities and investigated the competitive adsorption of CO_2 from gas mixtures [8]. Kim et al. studied methane separation from landfill gas using a six-step two-bed PSA process using CMS Takeda 3A [9]. Canevesi et al. researched a PSA process for biogas upgradation using a CMS adsorbent [10]. Two synthetic molecular sieves (5A and 13X) and a natural zeolite (clinoptilolite) as adsorbent materials were studied for the cleaning and upgrading of biogas by PSA with thermal desorption [11]. CO_2 separation using adsorption on 4A and 13X zeolite molecular sieves in dynamic conditions to upgrade landfill biogas was investigated by Montanari et al. [12]. Mofarahi and Shokroo compared the performance of zeolite 5A with that of zeolite 13X in oxygen separation from the air using a two-bed six-step PSA system through mathematical modeling [13]. Hauchhum and Mahanta investigated adsorption and regeneration behavior of CO_2 on zeolite 13X, zeolite 4A, and AC [14]. Shokroo et al. numerically investigated the performance of zeolite 5A and 13X in separating oxygen from air using a two-bed PSA system [15]. In addition, many studies have also been performed on the simulations of PSA

†To whom correspondence should be addressed.
E-mail: daehoko@hotmail.com, daeho.ko@gastopia.co.kr

processes [16-26].

The purpose of this study was to provide the necessary information for the selection of the adsorbent used in the vacuum pressure swing adsorption (VPSA) process by observing the performance influenced by the adsorbent as well as the design and operating conditions.

Therefore, this paper presents the investigation results of the performance of the VPSA process adopting CMS and zeolite 5A through simulations using gPROMS custom modeling software [27].

The next section introduces the target VPSA process and presents the adopted operating steps and VPSA mathematical simulation model [25,26], of which the novel point is in the simulation accuracy because the gas velocity within adsorption beds is precisely calculated using the mole balance equation, and the velocity strongly affects the exact prediction of the bed sizing, pressure drop, and performance, as explained in Ko's papers [25,26]. Simulation results are presented and discussed. In the final section, the comparison results are summarized and analyzed.

MATHEMATICAL SIMULATION MODEL

This study adopts the VPSA process and the simulation equations of Ko's papers [25,26], which introduce a novel method to calculate interstitial gas velocity within adsorption beds and prove the simulation model equations to be accurate by comparing the simulation results with pilot plant operation data and the commercial-scale vendor design data. The target process is the VPSA process consisting of a four-bed system with 12 operating steps, as explained by Ko [25,26]. The purpose of the VPSA process is to purify methane gas by the adsorption of carbon dioxide. The feed gas composition is 90% methane and 10% carbon dioxide. The operating steps are adsorption, pressure equalization, repose, blowdown, purge, pressure equalization, and pressurization, as described below and summarized in Table 1 [25,26].

In step 1, carbon dioxide is adsorbed on the adsorbent at high adsorption pressure in bed 1, while pressure is equalized between beds 3 and 4, that is, the gas is supplied from high-pressure bed 4 to low-pressure bed 3, and the blowdown step (regeneration of the adsorbent at atmospheric pressure) is carried out in bed 2. In the blowdown step, the gas within the adsorption bed is emitted into the tail gas stream without vacuum, while the valve above the bed is closed and that below the bed is opened.

In step 2, the carbon dioxide of bed 1 is continuously adsorbed on the adsorbent, and a part of the purified gas is provided to bed 3 from bed 1 to pressurize bed 3. The adsorbent is regenerated at vacuum pressure during the purge step of bed 2, and bed 4 is in a repose step. In the purge step, the gas is extracted using a vacuum pump, while the valve below the bed is opened and that above the bed is closed.

In step 3, beds 1 and 3 continue the same operations as in step 2, while bed 2 receives gas from bed 4 as the pressure equalization step.

In step 4, bed 1 provides the gas to bed 2 as the pressure equalization step, while bed 3 performs the adsorption step with the high adsorption pressure and bed 4 conducts the blowdown step with the atmospheric pressure.

In step 5, bed 1 is in the repose step, and vacuum regeneration of the adsorbent is performed at bed 4 as the purge step. Part of the purified gas from high-pressure bed 3 in the adsorption step flows into low-pressure bed 2 for pressurization.

In step 6, high-pressure bed 1 gives the gas to low-pressure bed 4 as the pressure equalization step, while bed 2 at the pressurization step receives the gas from bed 3 at the adsorption step.

In step 7, the blowdown step is carried out in bed 1, and the adsorption step is started at bed 2, while high-pressure bed 3 provides the gas to low-pressure bed 4 as the pressure equalization step.

In step 8, the vacuum purge step is performed at beds 1 and 4 at the pressurization step, which receives a part of the purified gas from bed 2 at the adsorption step, while bed 3 is in the repose step.

In step 9, low-pressure bed 1 obtains the gas from high-pressure bed 3 as the pressure equalization step, while part of the gas from high-pressure bed 2 at the adsorption step is transported into low-pressure bed 4 at the pressurization step.

In step 10, the gas of high-pressure bed 2 is moved into low-pressure bed 1 as the pressure equalization step, while beds 3 and 4 perform the blowdown and adsorption steps, respectively.

In step 11, bed 1 is pressurized by accepting the part of the purified gas from high-pressure bed 4 at the adsorption step, while bed 3 is purged with the vacuum pressure and bed 2 is in the repose step.

In step 12, beds 1 and 4 continuously conduct the pressurization and adsorption steps, respectively, while beds 2 and 3 carry out the pressure equalization step, that is, low-pressure bed 3 takes the gas from high-pressure bed 2.

The simulation model is formulated with the following assumptions [25,26].

(1) The Redlich-Kwong equation of state.

(2) No variable variations of radial direction.

(3) Nonisothermal and nonadiabatic conditions.

(4) Competitive adsorption behavior expressed as the Langmuir

Table 1. Operating step sequence of the VPSA process [25,26]

Step	1	2	3	4	5	6	7	8	9	10	11	12
Time(s)	10	120	10	10	120	10	10	120	10	10	120	10
Bed 1	AD	AD	AD	EQ1	RE	EQ2	BD	PG	EQ2	EQ1	PR	PR
Bed 2	BD	PG	EQ2	EQ1	PR	PR	AD	AD	AD	EQ1	RE	EQ2
Bed 3	EQ1	PR	PR	AD	AD	AD	EQ1	RE	EQ2	BD	PG	EQ2
Bed 4	EQ1	RE	EQ2	BD	PG	EQ2	EQ1	PR	PR	AD	AD	AD

AD=Adsorption; EQ=pressure equalization; RE=repose; BD=blow down; PG=purge; PR=pressurization

type isotherm.

(5) Temperature independent physical property of the bed.

(6) Ergun equation relating the gas velocity and the pressure drop within the bed.

(7) Linear driving force (LDF) model calculating the adsorption amount.

(8) The time-varying pressure profile at the boundary of the bed described by an exponential function of time [28].

Based on the above assumptions, the simulation model introduced in Ko's paper [25,26] was adopted as follows:

To calculate the adsorption equilibrium, the extended Langmuir isotherm is adopted:

$$q_i^* = \frac{q_{s,i} b_i P_i}{1 + \sum_{i=1}^{nc} b_i P_i} \tag{1}$$

where, P_i is the gas partial pressure.

The temperature (T) dependent parameters (q_s and b_i) are obtained using Eqs. (2.1) and (2.2), respectively:

$$q_{s,i} = q_{sa,i} + \frac{q_{sb,i}}{T} \tag{2.1}$$

$$b_i = b_{0,i} \exp\left(\frac{D_{E,i}}{T}\right) \tag{2.2}$$

The parameters ($q_{sa,i}$, $q_{sb,i}$, $b_{o,i}$, and $D_{E,i}$) are estimated using the isotherm measurement data.

The adsorption amount (q_i) is calculated using the LDF in Eq. (3).

$$\frac{\partial q_i}{\partial t} = k_i (q_i^* - q_i) \tag{3}$$

where, k_i is the mass transfer coefficient, called LDF coefficient.

The equation of state (EOS) (Eq. (4)) is adopted to obtain the concentration (C).

$$P = ZCRT \tag{4}$$

where, Z is the compressibility factor, R is the universal gas constant, and P is the gas pressure.

To calculate the component concentration C_i, Eq. (5) is used.

$$C_i = y_i C \tag{5}$$

The mole fraction (y_i) balance introduced by Ko [25] is expressed by Eq. (6.1)

$$-D_{ax}\left(\frac{\partial^2 y_i}{\partial z^2} + 2T\frac{\partial(1/T)}{\partial z}\frac{\partial y_i}{\partial z} + 2(1/P)\frac{\partial y_i}{\partial z}\frac{\partial P}{\partial z} + 2Z\frac{\partial(1/Z)}{\partial z}\frac{\partial y_i}{\partial z}\right) + u_I\frac{\partial y_i}{\partial z} + \frac{\partial y_i}{\partial t} + \frac{\rho_i RTZ(1-\varepsilon_{bed})}{P}\frac{1}{\varepsilon_{bed}}\left(\frac{\partial q_i}{\partial t} - y_i\sum_{i=1}^{nc}\frac{\partial q_i}{\partial t}\right) = 0 \tag{6.1}$$

Eq. (6.1) is derived by inserting the EOS ($y_iP=ZC_iRT$) into the component concentration balance in Eq. (6.2).

$$\frac{\partial C_i}{\partial t} + \frac{1-\varepsilon_{bed}}{\varepsilon_{bed}}\rho_s\frac{\partial q_i}{\partial t} - D_{ax}\frac{\partial^2 C_i}{\partial z^2} + \frac{\partial(u_I C_i)}{\partial z} = 0 \tag{6.2}$$

where, ε_{bed} is the bed void, ρ_s is the solid adsorbent density, D_{ax} is the axial dispersion coefficient, and z is the normalized axial distance in a bed from the feed inlet part.

The pressure drop is calculated using Ergun Eq. (7.1) when the interstitial gas velocity (u_I) is employed:

$$-\frac{\partial P}{\partial z} = 150\frac{(1-\varepsilon_{bed})^2}{\varepsilon_{bed}^2}\frac{\mu}{d_p^2}u_I + 1.75\frac{1-\varepsilon_{bed}}{\varepsilon_{bed}}\frac{\rho_g}{d_p}u_I|u_I| \tag{7.1}$$

Eq. (7.1) is derived by inserting the relation ($u_s=u_I\varepsilon_{bed}$) of the interstitial gas velocity and the superficial gas velocity (u_S) into the Ergun Eq. (7.2) using the superficial gas velocity [25,26].

$$-\frac{\partial P}{\partial z} = 150\frac{(1-\varepsilon_{bed})^2}{\varepsilon_{bed}^3}\frac{\mu}{d_p^2}u_S + 1.75\frac{1-\varepsilon_{bed}}{\varepsilon_{bed}^3}\frac{\rho_g}{d_p}u_S|u_S| \tag{7.2}$$

where, d_p is the adsorbent particle diameter, μ is the gas viscosity, and ρ_g is the gas density.

The interstitial gas velocity (u_I) is calculated using the molar flow rate ($\dot{n}$) within the adsorption bed (Eq. (8))

$$Pu_I A_{void} = Z\dot{n}RT \tag{8}$$

$$A_{void} = \varepsilon_{bed} A \tag{9}$$

where, A_{void} is the void cross-sectional area of the bed and A is the cross-sectional area of the inside of the adsorption bed.

The gas temperature within the bed is given by the gas energy balance in Eq. (10)

$$(\varepsilon_t\rho_g C_{pg} + \rho_{bed}C_{ps})\frac{\partial T}{\partial t} + \rho_g C_{pg}\varepsilon_{bed}u_I\frac{\partial T}{\partial z} - K_L\frac{\partial^2 T}{\partial z^2} - \rho_{bed}\sum_{i=1}^{nc}\Delta H_i\frac{\partial q_i}{\partial t} + \frac{2h_{Inside}}{R_{bed,\,Inside}}(T - T_{wall}) = 0 \tag{10}$$

where, ε_t is the total bed void fraction, C_{pg} is the gas heat capacity, ρ_{bed} is the bed bulk density packed with the adsorbent, C_{ps} is the solid adsorbent density, K_L is the effective axial thermal conductivity, ΔH_i is the isosteric heat of adsorption, h_{Inside} is the heat transfer coefficient inside the bed, $R_{bed,\,Inside}$ is the inside radius of the bed, and T_{wall} is the bed wall temperature.

The bed wall temperature is predicted by the wall energy balance in Eq. (11)

$$(\rho_w C_w)\pi(R_{bed,\,Outside}^2 - R_{bed,\,Inside}^2)\frac{\partial T_{wall}}{\partial t} = 2\pi R_{bed,\,Inside}h_{Inside}(T - T_{wall}) - 2\pi R_{bed,\,Outside}h_{Outside}(T_{wall} - T_{amb}) \tag{11}$$

where, ρ_w is the bed wall density, C_w is the heat capacity of the bed wall, $R_{bed,\,Outside}$ is the outside radius of the bed, and T_{amb} is the ambient temperature.

The mole balance Eq. (12.1) developed by Ko [25] is employed to calculate the molar flow rate.

$$\frac{\partial n}{\partial t} + (1-\varepsilon_{bed})\left(j\frac{L_{bed}}{N_D}\right)A\rho_s\sum_{i=1}^{nc}\frac{\partial q_i}{\partial t} + \left(\frac{\partial \dot{n}}{\partial z}\right)\left(j\frac{L_{bed}}{N_D}\right) = 0 \tag{12.1}$$

where, n is the mole number of the gas within the bed, $\dot{n}$ is the molar flow rate, L_{bed} is the packing bed length, N_D is the number of discretization in the finite difference method with respect to the bed axial domain, nc is the number of the gas components, and j is the parameter given as 1 or 2. For example, j is given as 1 when the forward finite difference method or backward finite difference method is adopted for the axial discretization, and j is set as 2 when

$$\frac{dC}{dt}=\left(-\frac{\partial \dot{n}}{\partial z}\right)\left(\frac{\Delta z}{\Delta V_{void}}\right)-\left(\sum_{i=1}^{nc}\frac{dq_i}{dt}\right)\rho_p \Leftrightarrow \frac{dn}{dt}=\dot{n}_{in}-\dot{n}_{out}-\left(\sum_{i=1}^{nc}\frac{dq_i}{dt}\right)\rho_s\left(j\Delta V_{solid}\right)$$
$$=-\left(\frac{d\dot{n}}{dz}\right)\left(j\Delta z\right)-\left(\sum_{i=1}^{nc}\frac{dq_i}{dt}\right)\left(\rho_s\right)\left(j\Delta V_{solid}\right)$$

When FFDM or BFDM is used, $j = 1$.
When CFDM is used, $j = 2$.

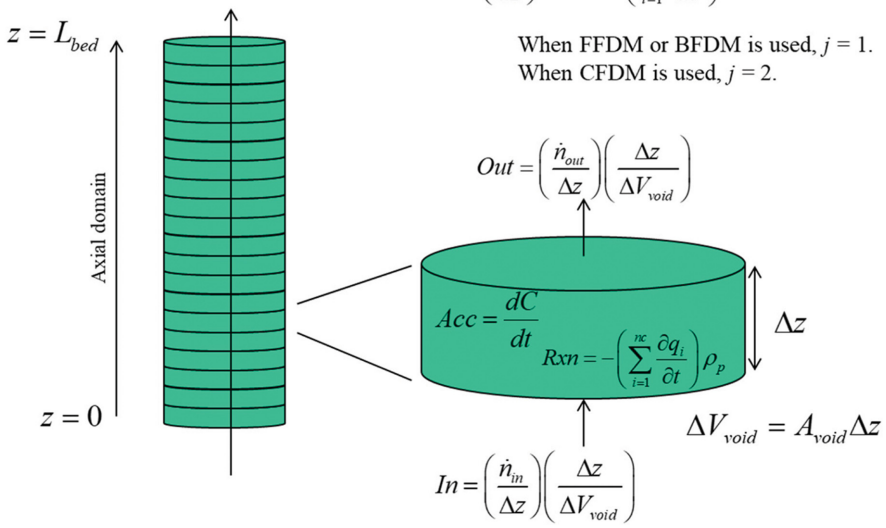

Fig. 1. The derivation method of the mole balance equation.

the centered finite difference method is employed for the axial discretization.

The derivation of the mole balance in Eq. (12.1) can be explained as follows:

The accumulation (Acc) consists of the inlet (In), outlet (Out), and reaction (Rxn) in the mole balance.

That is,

$$\mathrm{Acc}=\mathrm{In}-\mathrm{Out}\pm\mathrm{Rxn} \tag{12.2}$$

where, the concentration balance can be established (Eqs. (12.3)-(12.7)).

$$\mathrm{Acc}=\frac{\mathrm{dC}}{\mathrm{dt}} \tag{12.3}$$

$$\mathrm{In}=\left(\frac{\dot{\mathrm{n}}_{in}}{\Delta \mathrm{z}}\right)\left(\frac{\Delta \mathrm{z}}{\Delta \mathrm{V}_{void}}\right) \tag{12.4}$$

$$\mathrm{Out}=\left(\frac{\dot{\mathrm{n}}_{out}}{\Delta \mathrm{z}}\right)\left(\frac{\Delta \mathrm{z}}{\Delta \mathrm{V}_{void}}\right) \tag{12.5}$$

$$\mathrm{Rxn}=-\left(\sum_{i=1}^{nc}\frac{\partial \mathrm{q}_i}{\partial \mathrm{t}}\right)\rho_p \tag{12.6}$$

Therefore,

$$\frac{\mathrm{dC}}{\mathrm{dt}}=\left(-\frac{\partial \dot{\mathrm{n}}}{\partial \mathrm{z}}\right)\left(\frac{\Delta \mathrm{z}}{\Delta \mathrm{V}_{void}}\right)-\left(\sum_{i=1}^{nc}\frac{\mathrm{dq}_i}{\mathrm{dt}}\right)\rho_s \tag{12.7}$$

Eq. (12.7) can be reformulated as the mole balance in Eq. (12.8).

$$\frac{\mathrm{dn}}{\mathrm{dt}}=\dot{\mathrm{n}}_{in}-\dot{\mathrm{n}}_{out}-\left(\sum_{i=1}^{nc}\frac{\mathrm{dq}_i}{\mathrm{dt}}\right)\rho_s(\mathrm{j}\Delta \mathrm{V}_{solid})$$
$$=-\left(\frac{\mathrm{d}\dot{\mathrm{n}}}{\mathrm{dz}}\right)(\mathrm{j}\Delta \mathrm{z})-\left(\sum_{i=1}^{nc}\frac{\mathrm{dq}_i}{\mathrm{dt}}\right)\rho_s(\mathrm{j}\Delta \mathrm{V}_{solid}) \tag{12.8}$$

where, $\Delta \mathrm{z}=\frac{\mathrm{L}_{bed}}{\mathrm{N}_D}$ and $(1-\varepsilon_{bed})\left(\mathrm{j}\frac{\mathrm{L}_{bed}}{\mathrm{N}_D}\right)\mathrm{A}=\Delta \mathrm{V}_{solid}$

The development approach of the mole balance is summarized in Fig. 1.

The purity and recovery of methane are formulated using Eqs. (13) and (14):

$$\mathrm{Purity}_{CH_4,\,ave}(\%)=\frac{\int_0^{t_{AD}^{step01\sim03}}[\mathrm{y}_{CH_4}]_{z=L}\mathrm{dt}}{\mathrm{t}_{AD}^{step01\sim03}}\times 100 \tag{13}$$

$$\mathrm{Recovery}_{CH_4,\,ave}(\%)=\left(\frac{[\dot{\mathrm{n}}_{ave}^{step01}]_{z=L}[\mathrm{y}_{CH_4,\,ave}^{step01}]_{z=L}\mathrm{t}_{AD}^{step01}}{[\dot{\mathrm{n}}_{ave}^{step01\sim03}]_{z=0}\mathrm{y}_{feed,\,CH_4}\mathrm{t}_{AD}^{step01\sim03}}\right.$$
$$\left.+\frac{[\dot{\mathrm{n}}_{after\ split,\,ave}]_{z=L}[\mathrm{y}_{CH_4,\,ave}^{step02\sim03}]_{z=L}\mathrm{t}_{AD}^{step02\sim03}}{[\dot{\mathrm{n}}_{ave}^{step01\sim03}]_{z=0}\mathrm{y}_{feed,\,CH_4}\mathrm{t}_{AD}^{step01\sim03}}\right)\times 100 \tag{14}$$

The power consumption can be calculated by Eqs. (15)-(17).

Compressor power (J/s):

$$\mathrm{Power}_{Comp,\,ave}=\frac{\int_0^{t_{AD}}\left[\dot{\mathrm{n}}_{feed}\mathrm{RT}_{z=0}\frac{\gamma}{\gamma-1}\left(\left(\frac{\mathrm{P}_{AD}}{\mathrm{P}_{atm}}\right)^{\frac{\gamma-1}{\gamma}}-1\right)\right]}{\mathrm{t}_{AD}} \tag{15}$$

Vacuum pump power (J/s):

$$\mathrm{Power}_{VP,\,ave}=\frac{\int_0^{t_{PG}}\left[\dot{\mathrm{n}}_{PG}\mathrm{RT}_{z=0}\frac{\gamma}{\gamma-1}\left(\left(\frac{\mathrm{P}_{z=0}}{\mathrm{P}_{PG}}\right)^{\frac{\gamma-1}{\gamma}}-1\right)\right]}{\mathrm{t}_{PG}} \tag{16}$$

Total specific power (J/mol/s):

$$\mathrm{Power}_{SP,\,ave}=\frac{\mathrm{Power}_{comp,\,ave}+\mathrm{Power}_{VP,\,ave}}{(\dot{\mathrm{n}}_{prod})(\mathrm{Purity}_{CH_4}/100)} \tag{17}$$

The boundary conditions of each operating step are introduced in

Table 2. Adsorption isotherm parameters

Adsorbent	Carbon molarcular sieve (CMS) [25,26]		Zeolite 5A [29]	
Component	CH_4	CO_2	CH_4	CO_2
q_{sa} (mole kg^{-1})	−1.8	0.4	−10.8616	0.109987
q_{sb} (mole K kg^{-1})	1,502	93.74	4,097.86	126.66
b_0 (bar^{-1})	0.413302326	0.000755814	163.255	845.633
D_E (K)	−238	2,250.1	−1,934.61	−1,419.54

Table 3. Basic condition for the comparison study of adsorbents for Figs. 2-7

Variables	Values
Packing bed Length (m)	1
Inside bed radius (m)	0.13
Adsorption Pressure (P_{AD}) from Step 1 through Step 3 (Pa)	10^6
Blowdown Pressure (P_{BD}) at Step 7 (Pa)	10^5
Purge Pressure (P_{PG}) at Step 8 (Pa)	10^4

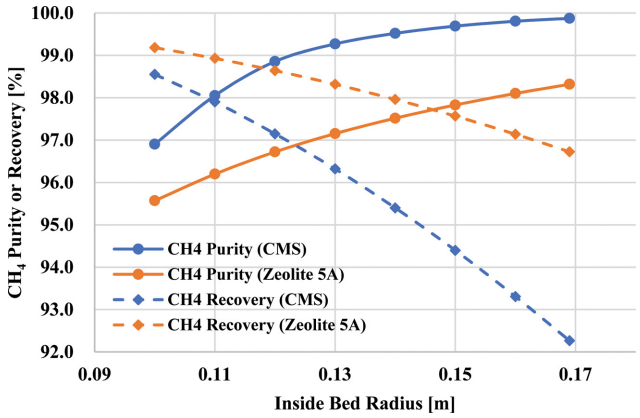

Fig. 2. The effect of bed radius on methane purity and recovery.

Ko's paper [25]:

This paper presents the performance comparison results of CMS and zeolite 5A through cyclic dynamic simulations from the first cycle to the cyclic steady state (CSS). In the current simulation models, the 100% methane gas initially fills the bed, and the CSS is determined when the value of the CSS_{check} variable, as shown in Eq. (18) [25] is less than 0.01 because the VPSA performance must be checked at the CSS.

$$\begin{aligned} CSS_{check} = & \sum_{i=1}^{nc}\sum_{k=1}^{N_p+1}\left|q_{i,\,t=0,\,k} - q_{i,\,t=t_{cycle},\,k}\right| \\ & + \sum_{k=2}^{N_p}\left|y_{CH_4,\,t=0,\,k} - y_{CH_4,\,t=t_{cycle},\,k}\right| \\ & + \sum_{k=2}^{N_p}\left|T_{t=0,\,k} - T_{t=t_{cycle},\,k}\right| \\ & + \sum_{k=2}^{N_p}\left|T_{wall,\,t=0,\,k} - T_{wall,\,t=t_{cycle},\,k}\right| \end{aligned} \quad (18)$$

The estimated adsorption isotherm parameters are listed in Table 2. The parameter values of CMS are from Ko's paper [25,26], and

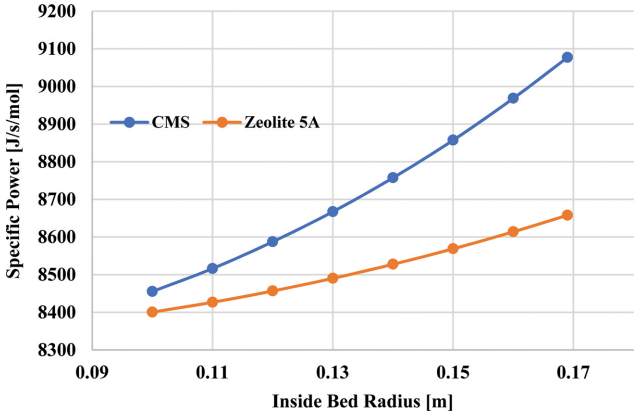

Fig. 3. The effect of bed radius on specific power.

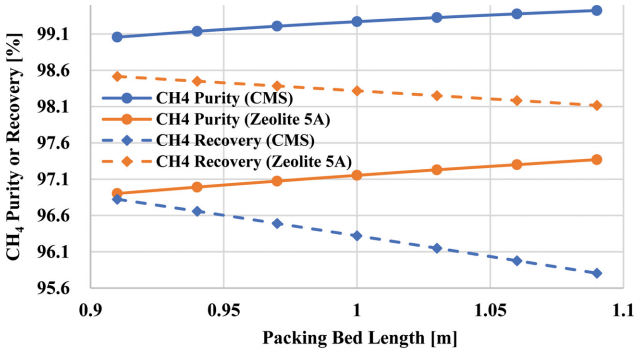

Fig. 4. The effect of bed length on methane purity and recovery.

those of zeolite 5A were estimated using data from Ahn's Master's thesis [29].

RESULTS AND DISCUSSION

This study presents the effects of vacuum purge pressure, adsorption pressure, bed length, and bed radius on the VPSA performance, such as the methane purity and recovery, and the specific power of the CMS and zeolite 5A as adsorbents.

Table 3 shows the basic condition of the VPSA process.

Figs. 2-5 illustrate the effects of the inside bed radius and bed length on the methane purity and recovery, and the specific power, respectively. For example, in Figs. 2-3, the value of the radius is changed while the other variables (bed length and pressure) of Table 3 are constant.

The methane purity and specific power are proportional to the bed radius and bed length, while methane recovery is inversely

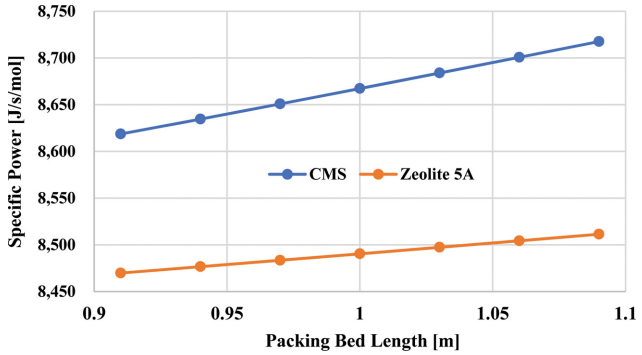

Fig. 5. The effect of bed length on specific power.

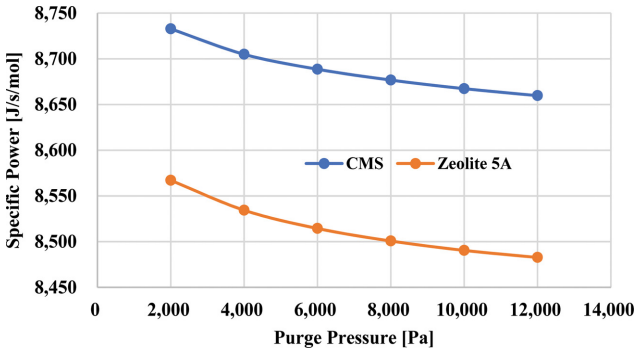

Fig. 7. The effect of vacuum purge pressure on specific power.

proportional to them. This is because increasing the bed radius or length leads to an increase in the gas contact time (t_{cont}) with the adsorbents.

The contact time is the bed length (L_{bed}) divided by the interstitial gas velocity (Eq. (19)). The bed area affects the interstitial gas velocity. That is, when the bed radius increases with a given flow rate, the interstitial gas velocity decreases (Eq. (20)), which increases the contact time (Eq. (19)). In addition, when the bed length increases with the given flow rate and bed radius, the contact time increases.

$$t_{cont} = L_{bed}/u_I \tag{19}$$

$$\dot{V} = u_I A_{void} = u_I A \varepsilon_b \tag{20}$$

The longer the contact time, the higher the product purity and the lower the recovery. Thus, much more carbon dioxide is adsorbed on the adsorbent, leading to higher methane purity, and a little more methane is also adsorbed on the adsorbent with the longer contact time, resulting in lower methane recovery. The mass transfer zone with a longer contact time must be located in the lower part of the adsorption bed than that with a shorter contact time. Therefore, if the product gas in VPSA processes is required to have high purity, a longer contact time must be taken by increasing the bed diameter or inside bed radius, or decreasing the feed flow rate. The specific power increases with the gas contact time because the recovery decreases with time.

When the adsorption pressure is high (P_{AD}=10^6 Pa), CMS is better than zeolite 5A in terms of methane purity; however, zeolite 5A is better than CMS in terms of methane recovery and specific power.

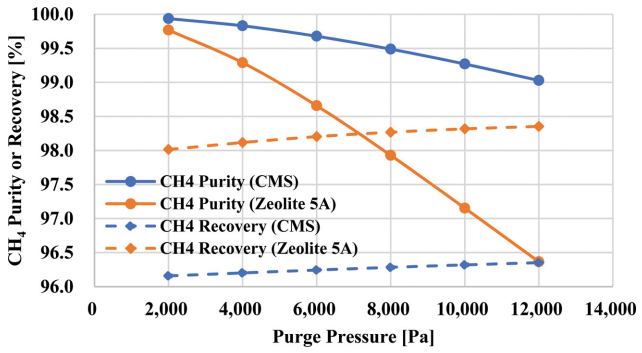

Fig. 6. The effect of vacuum purge pressure on methane purity and recovery.

The purge pressure effects on the VPSA performance are described in Figs. 6-7.

The lower the purge pressure using a vacuum pump, the higher the methane purity obtained. Methane purity using zeolite 5A is more sensitive to purge pressure than that using CMS. This is due to the isotherm characteristics of zeolite 5A. This means that the carbon dioxide adsorption equilibrium of zeolite 5A increases more sharply as the pressure increases at a low vacuum pressure range compared to that of CMS.

The methane purity when CMS is adopted is higher than that when zeolite 5A is employed; however, the methane recovery using zeolite 5A is higher than that using CMS. The higher the purge pressure, the higher is the methane recovery. Consequently, the specific power could be reduced if zeolite 5A was used. The design condition decision is based on factors such as product gas specification, required power consumption, and product flow rate. For example, vacuum purge pressure using zeolite 5A can be selected as 2,000 Pa to obtain high methane purity (99.77%), high methane recovery (98.01%), and comparatively low specific power (8,567 J/s/mol).

The basic conditions for analyzing the effect of the low adsorption pressure (250,000-600,000 Pa) on the performance are shown in Table 4. The investigation results of the adsorption pressure effects on the performance are shown in Figs. 8-9. For instance, in Figs. 8-9, the value of the adsorption pressure is changed, while the variables of the bed length, the inside bed radius, and the purge pressures of Table 4 are constant.

When the VPSA processes are operated at a low adsorption pressure ranging from 250,000 to 600,000 Pa with a vacuum purge pres-

Table 4. Basic condition for the comparison study of adsorbents for Figs. 8-9

Variables	Values
Packing bed length (m)	1
Inside bed radius (m)	0.13
Purge pressure (P_{PG}) at Step 8 (Pa)	10^3

Blowdown step (step 7) is excluded, that is to say, blowdown step time is changed from 10 s to 0 s, and purge step time is from 120 s to 130 s.

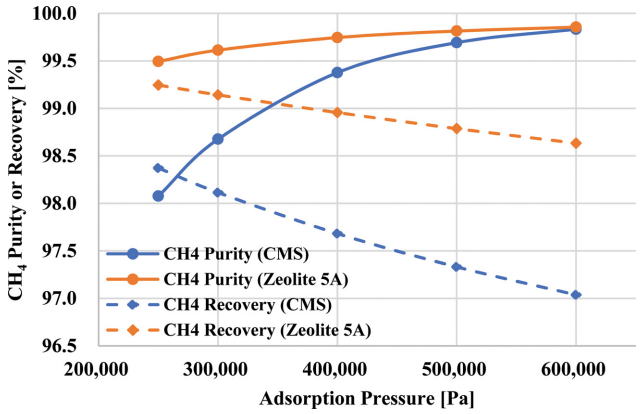

Fig. 8. The effect of adsorption pressure (2.5-6 bar) on methane purity and recovery.

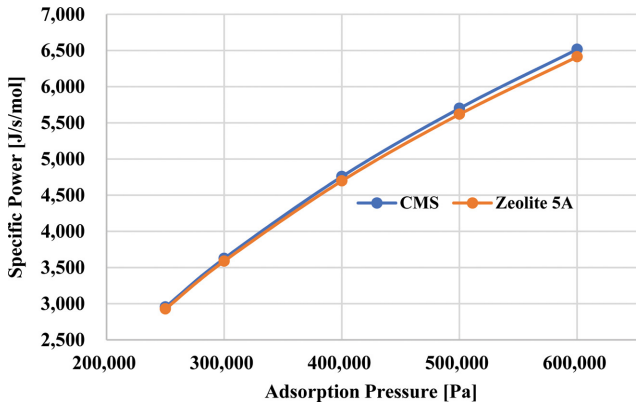

Fig. 9. The effect of adsorption pressure (2.5-6 bar) on specific power.

sure of 1,000 Pa, the performance resulting from using zeolite 5A is better than that using CMS. The specific power of zeolite 5A is slightly lower than that using CMS.

Thus, to save the specific power and to obtain high methane purity and recovery, a low-pressure operation adopting zeolite 5A is preferable. If 250,000 Pa and 1,000 Pa are selected as the adsorption pressure and purge pressure, respectively, the performance using zeolite 5A is 99.49% methane purity, 99.25% methane recovery, and 2,928 J/s/mol specific power, while that using CMS is 98.08% methane purity, 98.37% methane recovery, and 2,953.5 J/s/mol.

The current investigation results, including the sensitivity analysis based on the demo plant scale (feed flow rate=100 Nm^3/h) can be used to determine the design conditions of a real commercial-scale plant if the following are kept in mind:

(1) The adsorption bed size and adsorbent amount are proportional to the feed flow rate.

(2) The gas contact time with the adsorbent is proportional to the bed radius and bed length and inversely proportional to the feed gas flow rate.

(3) The operating step sequence and times adopted in this study can be used for full-scale plants.

(4) The operating pressures of the current demo plant scale can be the same as those of the full-scale plant if the gas contact times are the same.

For example, if the inside bed volume at a feed flow rate of 100 Nm^3/h is 0.053 m^3 ($=\pi\times(0.13\ m)^2\times 1\ m$), the volume at a feed flow rate of 1,000 Nm^3/h can be determined as 0.53 m^3. Thus, the bed radius and bed length at a feed flow rate of 1,000 Nm^3/h can be determined as 0.4107 m and 1 m, respectively. This is because the bed size is affected by the gas contact time.

CONCLUSIONS

Two adsorbents (CMS and zeolite 5A) were compared with respect to the VPSA performance at CSS through cyclic dynamic simulations. The simulations were carried out from the first cycle, at which 100% methane gas initially filled the bed, to the CSS. At CSS, the values of the variables such as the gas temperature, gas mole fractions, and adsorption amount at the start time of the CSS are the same as those at the end time of the CSS.

The target process adopts the four-bed twelve-operating step VPSA process of Ko's paper [25,26] to separate methane and carbon dioxide mixture gas. The feed gas consists of 90% methane and 10% carbon dioxide. This work also employs the mathematical formulation of Ko's paper [25,26], which made it possible to calculate the exact interstitial gas velocity within the adsorption bed by deriving the mole balance equation. Accurate gas velocity calculation is crucial in determining the optimal VPSA process conditions, such as the adsorption bed size and the gas contact time affected by the operating step times, and flow rates of the feed gas and the purge gas. Thus, the simulation model was validated well enough to be used in predicting the performance of the VPSA process, as explained in Ko's papers [25,26]. The performance in this study includes methane purity, methane recovery, and specific power.

When a high adsorption pressure (10^6 Pa) and vacuum purge pressure ranging from 2.0×10^3 to 1.2×10^4 Pa are adopted, the CMS adsorbent has an advantage over zeolite 5A in terms of methane purity, while zeolite 5A is better than CMS in terms of methane recovery and specific power, as described in Figs. 1-6.

However, if the low-pressure operating condition is employed, that is, a low adsorption pressure ranging from 2.5×10^5 to 6.0×10^5 Pa and a low vacuum purge pressure of 10^3 Pa, the zeolite 5A is superior to the CMS in terms of methane purity, methane recovery, and specific power. This is because the zeolite 5A isotherm shows that the adsorption equilibrium amount increases more rapidly with increasing pressure in the vacuum pressure range; however, the CMS isotherm does not.

The best VPSA design conditions and proper selection of adsorbents depend on situations such as product specifications, power constraints, and the environment. For example, the effect of humidity of the feed gas stream on the adsorbents must be considered when selecting the adsorbent because, generally, zeolite-type adsorbents are very vulnerable to humidity, and CMS may be preferred in humid weather conditions. Of course, filter installation before the adsorption beds would be desirable to remove the moisture in the feed gas stream and prevent the adsorbent from performance degradation in the industry. The major contribution of this study is to show the necessary information for proper adsorbent selection according to the design and operating conditions of the VPSA

process through accurate dynamic cyclic simulations instead of a large number of experiments. In summary, at high operating pressure, CMS is better than zeolite 5A for methane purity and zeolite 5A is better for methane recovery and specific power; however, at low operating pressure, zeolite 5A has advantages over CMS in terms of methane purity, recovery, and specific power.

Thus, the results of this study will be useful for choosing the proper adsorbent and determining the optimal design conditions for the VPSA process.

NOMENCLATURE

A : cross sectional area within bed [m^2]
A_{void} : void cross sectional area within bed [m^2]
b_i : Langmuir constant [1/bar] as a function of temperature
$b_{o,i}$: Langmuir isotherm parameters [1/bar]
C : total concentration [mol/m^3]
C_i : concentration of component *i* [mol/m^3]
C_{pg} : heat capacity of gas [J/(kg K)]
C_{ps} : heat capacity of adsorbent [J/(kg K)]
C_w : heat capacity of bed wall [J/(kg K)]
CSS_{check} : criterion variable for the CSS determination
D_{ax} : axial dispersion coefficient [m^2/s]
$D_{E,i}$: isotherm parameters [K]
d_p : adsorbent particle diameter [m]
ΔH_i : isosteric heat of adsorption [J/mol]
h_{Inside} : heat transfer coefficient of inside the bed [J/(m^2 s K)]
$h_{Outside}$: heat transfer coefficient of outside the bed [J/(m^2 s K)]
j : 1 when forward finite difference method (FFDM) or backward finite difference method (BFDM) is used for axial discretization; 2 when centered finite difference method (CFDM) is used for axial discretization
k_i : mass transfer coefficient of linear driving force (LDF) model of component *i* [1/s]
K_L : effective axial thermal conductivity [J/(m s K)]
L_{bed} : packing bed length [m]
$\dot{n}$: molar flow rate [mol/s]
$\dot{n}_{feed}$: feed gas molar flow rate [mol/s]
$\dot{n}_{PG}$: purge gas molar flow rate [mol/s]
$\dot{n}_{prod}$: product gas molar flow rate [mol/s]
$\dot{n}^{Step(K)}$: molar flow rate at step K [mol/s]
$\dot{n}^{Step(K)}_{ave}$: average molar flow rate during step K [mol/s]
$\dot{n}_{after\ split,\ ave}$: average molar flow rate in product stream after splitting [mol/s]
nc : number of component
N_D : number of discretization in finite difference method as to the bed axial domain
P : total pressure [Pa]
P_i : partial pressure [Pa]
P_{AD} : adsorption pressure [Pa]
P_{BD} : blowdown pressure [Pa]
P_{PG} : purge pressure [Pa]
$Purity_{CH_4}$: methane purity [%]
$Recovery_{CH_4}$: methane recovery [%]
$Power_{Comp,ave}$: average compressor power [J/s]
$Power_{VP,ave}$: average vacuum pump power [J/s]
$Power_{SP,ave}$: total average specific power [J/(mol s)]
R : universal gas constant [J/(mol K)]
q_i : adsorbed amount of component *i* [mol/kg]
q_i^* : equilibrium amount adsorbed of component *i* [mol/kg]
q_s : equilibrium parameter for extended Langmuir isotherm [mol/kg]
$q_{sa,i}$: Langmuir isotherm parameters [mol/kg]
$q_{sb,i}$: Langmuir isotherm parameters [mol K/kg]
$R_{bed,inside}$: inside radius of the bed [m]
$R_{bed,outside}$: outside radius of the bed [m]
t_{AD} : adsorption operating step time [s]
$t_{AD}^{Step(K)}$: operating time of step K (adsorption) [s]
t_{PG} : purge operating step time [s]
T : gas temperature [K]
T_{wall} : bed wall temperature [K]
T_{amb} : ambient temperature [K]
u_I : interstitial gas velocity [m/s]
y_i : mole fraction of component *i*
$y_{feed,i}$: feed mole fraction of component *i*
$y_i^{Step(K)}$: mole fraction of component *i* at step K
$y_{i,ave}^{Step(K)}$: average mole fraction of component *i* at step K
z : normalized axial distance in bed from the feed inlet
Z : compressibility factor

Greek Letters

μ : gas viscosity [kg/(m s)]
ε_{bed} : bed void
ε_t : total bed void fraction
ρ_{bed} : bed density [kg/m^3]
ρ_g : gas density [kg/m^3]
ρ_s : solid density [kg/m^3]
ρ_w : wall density [kg/m^3]

REFERENCES

1. J. G. Lu, M. D. Cheng, Y. Ji and Z. Hui, *J. Fuel Chem. Technol.*, **37**(6), 740 (2009).
2. N. Casas, J. Schell, L. Joss and M. Mazzotti, *Sep. Purif. Technol.*, **104**, 183 (2013).
3. M. Zaman and J. H. Lee, *Korean J. Chem. Eng.*, **30**(8), 1497 (2013).
4. W. Sun, Y. Shen, D. Zhang, H. Yang and H. Ma, *Ind. Eng. Chem. Res.*, **54**(30), 7489 (2015).
5. E. S. Kikkinides, R. T. Yang and S. H. Cho, *Ind. Eng. Chem. Res.*, **32**(11), 2714 (1993).
6. K. T. Chue, J. N. Kim, Y. J. Yoo, S. H. Cho and R. T. Yang, *Ind. Eng. Chem. Res.*, **34**, 591 (1995).
7. J.-G. Jee, S.-J. Lee, H.-M. Moon and C.-H. Lee, *Adsorption*, **11**, 415 (2005).
8. R. V. Siriwardane, M.-S. Shen and E. P. Fisher, *Energy Fuels*, **17**(3), 571 (2003).
9. M.-B. Kim, Y.-S. Bae, D.-K. Choi and C.-H. Lee, *Ind. Eng. Chem. Res.*, **45**(14), 5050 (2006).
10. R. L. S. Canevesi, K. A. Andreassen, E. A. da Silva, C. E. Borba and C. A. Grande, *Ind. Eng. Chem. Res.*, **57**(23), 8057 (2018).

11. A. Alonso-Vicario, J. R. Ochoa-Gómez, S. Gil-Río, O. Gómez-Jiménez-Aberasturi, C. A. Ramírez-López, J. Torrecilla-Soria and A. Domínguez, *Micropor. Mesopor. Mater.*, **134**(1-3), 100 (2010).
12. T. Montanari, E. Finocchio, E. Salvatore, G. Garuti, A. Giordano, C. Pistarino and G. Busca, *Energy*, **36**(1), 314 (2011).
13. M. Mofarahi and E. J. Shokroo, *Pet. Coal*, **55**(3), 216 (2013).
14. L. Hauchhum and P. Mahanta, *Int. J. Energy Environ. Eng.*, **5**, 349 (2014).
15. E. J. Shokroo, D. J. Farsani, H. K. Meymandi and N. Yadollahi, *Korean J. Chem. Eng.*, **33**(4), 1391 (2016).
16. S. P. Knaebel, D. Ko and L. T. Biegler, *Adsorption*, **11**, 615 (2005).
17. L. Jiang, L. T. Biegler and V. G. Fox, *AIChE J.*, **49**(5), 1140 (2003).
18. L. Jiang, V. G. Fox and L. T. Biegler, *AIChE J.*, **50**(11), 2904 (2004).
19. L. Jiang, L. T. Biegler and V. G. Fox, *Comput. Chem. Eng.*, **29**, 393 (2005).
20. D. Ko, R. Siriwardane and L. T. Biegler, *Ind. Eng. Chem. Res.*, **42**(2), 339 (2003).
21. D. Ko, R. Siriwardane and L. T. Biegler, *Ind. Eng. Chem. Res.*, **44**(21), 8084 (2005).
22. D. Nikolic, A. Giovanoglou, M. C. Georgiadis and E. S. Kikkinides, *Ind. Eng. Chem. Res.*, **47**(9), 3156 (2008).
23. A. Agarwal, L. T. Biegler and S. E. Zitney, *Ind. Eng. Chem. Res.*, **48**(5), 2327 (2009).
24. S. Kim, D. Ko and I. Moon, *Ind. Eng. Chem. Res.*, **55**(48), 12444 (2016).
25. D. Ko, *Ind. Eng. Chem. Res.*, **55**(33), 8967 (2016).
26. D. Ko, *Ind. Eng. Chem. Res.*, **55**(4), 1013 (2016).
27. Process Systems Enterprise, gPROMS, 1997-2017, www.psenterprise.com/gPROMS.
28. J. A. Delgado and A. E. Rodrigues, *Chem. Eng. Sci.*, **63**, 4452 (2008).
29. E.-A. Ahn, *A study on experiments and simulations of PSA processes for hydrogen separation from reforming gas*, Master Dissertation, Korea University, Republic of Korea (2006).